Acta Crystallographica Section B
Structural Science
ISSN 0108-7681

Energetic materials: α-NTO crystallizes as a four-component triclinic twin

Nadezhda Bolotina,‡ Kristin Kirschbaum and A. Alan Pinkerton*

Department of Chemistry, University of Toledo, Toledo, OH 43606, USA

‡ Permanent address: Institute of Crystallography, Moscow, Russia; e-mail: bolotina@ns.crys.ras.ru.

Correspondence e-mail: apinker@uoft02.utoledo.edu

Received 2 May 2005
Accepted 15 July 2005

The prevalent polymorph of the energetic material 5-nitro-2,4-dihydro-1,2,4,-triazol-3-one, α-NTO, crystallizes as a four-component twin with triclinic symmetry (space group $P\bar{1}$). All crystals under investigation were fourlings, *i.e.* they contained each of the four possible twin components. Complete data sets were collected for two crystals, one with a predominant amount of one individual component (55%) and one with approximately equal volumes of each component. In both cases the fourling components are related by the twofold axes inherent in the holohedral symmetry of a pseudo-orthorhombic superlattice with $\mathbf{a}_o = \mathbf{a}_t$, $\mathbf{b}_o = \mathbf{b}_t$ and $\mathbf{c}_o = \mathbf{a}_t + \mathbf{b}_t + 2\mathbf{c}_t$. The triclinic unit cell contains four crystallographically independent planar molecules in the asymmetric unit, each of which forms a hydrogen-bonded flat chain parallel to $\mathbf{a}_t$. Pairs of chains are combined into planar ribbons by additional hydrogen bonds. Thus, two independent ribbons extend parallel to $\mathbf{a}_t$, creating a dihedral angle of $\sim 70^\circ$. The origin of the twinning is derived from consideration of the crystal packing and the hydrogen-bonding scheme.

1. Introduction

NTO (5-nitro-2,4-dihydro-1,2,4,-triazol-3-one) and its derivatives have been known since 1905[1] and the explosive nature of one of the NTO derivatives was recognized early on (Manchot & Noll, 1905). Over the next 80 years there was not much interest in NTO beyond its synthesis and reactivity (Chipen *et al.*, 1966; Kröger *et al.*, 1969; Gehlen & Schmidt, 1965; Kofman *et al.*, 1980) until the recognition of the explosive properties of NTO itself (Lee *et al.*, 1987; Lee & Coburn, 1988) initiated extensive chemical, physical and theoretical studies. Of particular interest is the high energy of this material combined with low or relatively low thermal, radiation, impact and spark sensitivity. Thorough reviews on the chemistry and decomposition mechanisms of NTO (Singh *et al.*, 2001), the syntheses, characterization and thermolyses of more than 50 NTO salts (Singh & Felix, 2002), and also the crystal structures and applications of NTO and its salts (Singh & Felix, 2003) have been published over the last 4 years.

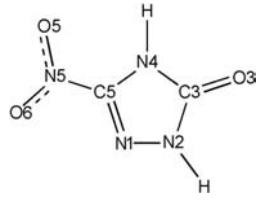

[1] It was originally identified as the 3-hydroxy tautomer.

Table 1
Unit-cell transformations for the α-NTO crystal (see also Table 2).

	Cell 1	Cell 2	Cell 3	Cell 4	Cell 5
Basis	**a**, **b**, **c**	**a**, $-$**b**, $-$**a** $-$ **c**	$-$**a**, **b**, $-$**b** $-$ **c**	$-$**a**, $-$**b**, **a** + **b** + **c**	**a**, **b**, **a** + **b** + 2**c**
a (Å)	5.1233	5.1233	5.1233	5.1233	5.1233
b (Å)	10.314	10.314	10.314	10.314	10.314
c (Å)	17.998	18.031	18.005	18.031	34.143
α (°)	106.61	106.62	106.68	106.62	89.98
β (°)	97.81	98.54	97.88	98.46	89.65
γ (°)	90.13	89.87	89.87	90.13	90.13

Surprisingly, the discovery of a second solid polymorph of NTO (Lee & Gilardi, 1993), the metastable β-form, in addition to the stable, dominant α-form, has received relatively little attention outside the structural community. While several research groups are studying crystallization conditions for energetic materials (see *e.g.* review: van der Heijden, 1998, and references therein; Kim & Kim, 2001; Mathieu *et al.*, 2001; van der Heijden & Bouma, 2004; Cai & Deng, 2004), investigations into the systematic development of crystallization conditions that support the synthesis of reasonable amounts of the β-polymorph or of the pure α-form have yet to be initiated.

Lee and Gilardi reported the simultaneous crystallization of the α- and β-phases from an aqueous solution of NTO. Identification of the two different polymorphs was performed by single-crystal crystallography, IR spectroscopy and X-ray powder diffraction patterns. In our hands, the resulting ratio of α:β phases was approximately 98:2, as estimated from optical microscopy based on the different morphology of the two phases.

The crystal structure of the metastable β-NTO phase could be accurately determined (R_1 = 0.05), but attempts to find a final satisfying structural model for α-NTO were unsuccessful. Although the unit-cell parameters, the space group $P\bar{1}$ [2] and the position of the molecules in the unit cell could be resolved, the recognized but unsolved twinning problem (Lee & Gilardi, 1993; Gilardi & Flippen-Anderson, 2002) prevented the determination of accurate atomic coordinates (R_1 = 0.17) for this phase.

Consequently, until now β-NTO was used in studies such as the calculation of crystal lattice energy which require the knowledge of accurate structural data (Xiao *et al.*, 2004; Sorescu & Thompson, 1997; Sorescu *et al.*, 1996; Zhurova & Pinkerton, 2001; Bolotina *et al.*, 2003), whereas solid-state investigations on radiation damage (Beard & Sharma, 1989), impact studies (Franken *et al.*, 1999) and the interpretation of vibration spectra (Hiyoshi *et al.*, 2004) were based on the predominant α-polymorph.

However, several of the investigated physical properties of explosive materials depend on crystal packing, hydrogen bonding, lattice energy or density, properties that are determined by the crystal structure and are therefore different for the α- and β-NTO polymorphs. The density, for example, is an important factor in the evaluation of the velocity of detonation of energetic materials (*e.g.* Rothstein & Petersen, 1979) and the description of crystal orientation for impact studies can be problematic in the case of a twinned crystal.

Herein we report a detailed analysis of the twinning of α-NTO, as well as the structural parameters from a fully refined model.

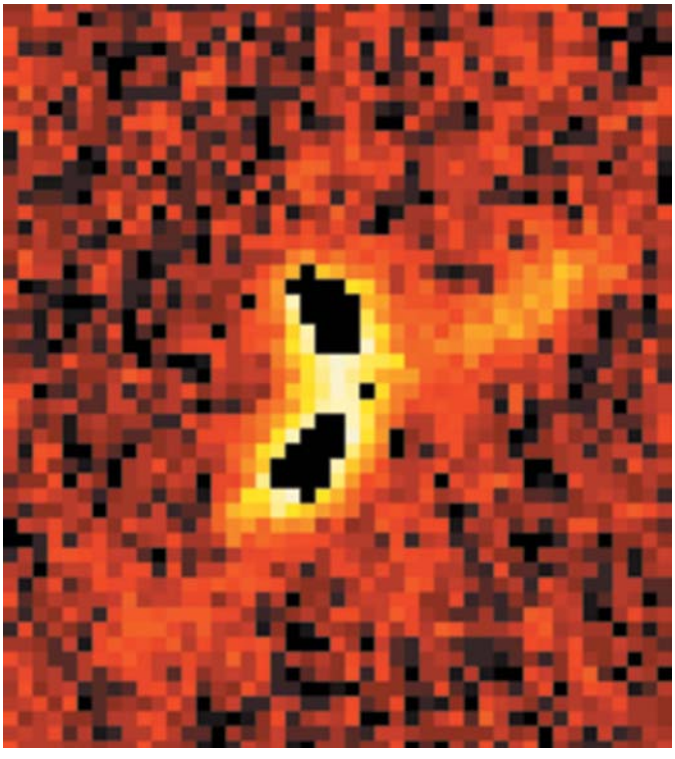

Figure 1
Example of a split diffraction profile.

2. Experimental

Experiments on two different crystals obtained from aqueous solution will be described. Initially, a parallelepiped-shaped crystal of α-NTO, 0.34 × 0.26 × 0.20 mm^3, was used for the X-ray structure investigation. Data collection was carried out at room temperature with a Bruker Platform diffractometer equipped with a SMART 1K-CCD detector, a normal-focus Mo $K\alpha$ tube and graphite monochromator. The crystal was mounted on a glass capillary with epoxy resin. 0.3° ω-scans were performed at four φ-settings with $2\theta = -28°$ at a detector distance of 5 cm. Although many diffraction profiles looked like reflections originating from a single or merohedrally twinned crystal, others seemed to be partially overlapped or even clearly split (Fig. 1). However, all reflections could be indexed using either one of four possible orientation matrices based on a triclinic unit cell (Table 1). The crystal data were treated as if originating from a pseudo-merohedral twin using

[2] The space group was correctly determined to be $P\bar{1}$, not $P1$ as cited in several publications.

Table 2
Crystal data and structure refinement for α-NTO.

	Crystal (1)		Crystal (2)	
Empirical formula	$C_2H_2N_4O_3$		$C_2H_2N_4O_3$	
Formula weight	130.08		130.08	
Temperature (K)	298 (1)		298 (1)	
Wavelength (Å)	0.71073		0.71073	
Crystal system	Triclinic		Triclinic	
Space group	$P\bar{1}$		$P\bar{1}$	
Z	8		8	
Density (calculated) (Mg m^{-3})	1.916		1.916	
Absorption coefficient (mm^{-1})	0.178		0.178	
F(000)	528		528	
Unit-cell lengths (Å)	a = 5.1233 (8)		a = 5.1316 (2)	
	b = 10.314 (2)		b = 10.3276 (4)	
	c = 17.998 (3)		c = 18.0345 (8)	
Unit cell angles (°)	α = 106.610 (2)		α = 106.637 (2)	
	β = 97.810 (2)		β = 98.088 (2)	
	γ = 90.130 (2)		γ = 90.021 (2)	
Volume (Å^3)	902.1 (2)		905.8 (1)	
Crystal size (mm^3)	0.34 × 0.26 × 0.20		0.24 × 0.24 × 0.30	
θ range for data collection (°)	2.06–28.70		1.19–28.12	
Index ranges	$-6 \le h \le 6$		$-6 \le h \le 6$	
	$-13 \le k \le 13$		$-13 \le k \le 13$	
	$-24 \le l \le 23$		$-23 \le l \le 23$	
Crystal–detector distance (cm)	5		15	
Data collected/$I > 2\sigma(I)$/ parameters	8966/8202/328		6208/6032/328	
Ratio of twin components (%)	54.9 (1), 9.1 (1), 20.2 (1), 15.8 (1)		27.1 (1), 19.3 (1), 28.6 (1), 25.0 (1)	
	SHELXTL	*JANA*2000	*SHELXTL*	*JANA*2000
Goodness-of-fit	1.122	1.00	1.131	0.99
Final R indices [$I > 2\sigma(I)$]	R_1 = 0.043	R_1 = 0.070	R_1 = 0.036	R_1 = 0.060
R indices (all data)	R_1 = 0.048	R_1 = 0.072	R_1 = 0.037	R_1 = 0.061

a fixed large integration box (1.9 × 1.9 × 0.9°) to obtain the total intensity of reflections originating from all twin components (*SAINT*; Bruker, 2001). These data were used to obtain a preliminary structure solution (*SHELXTL*; Bruker, 2000*a*). As expected from the literature (Lee & Gilardi, 1993; Gilardi & Flippen-Anderson, 2002), no satisfactory refinement was obtained at this point. However, determination of the twin laws (see below) and appropriate refinement resulted in an adequate model that described the crystal as a fourling with four discrete components in differing amounts (Table 2). An additional experiment was performed using a second crystal of α-NTO. In this case a Bruker platform diffractometer was used equipped with a SMART 6000 CCD detector (fine-focus Mo tube, graphite monochromator). The second crystal was 0.24 × 0.24 × 0.30 mm^3 in size and regularly shaped. Data were collected with 0.3° ω-scans at four φ-settings, two 2θ settings of −15 and −40° and a long 15 cm crystal–detector distance in an attempt to resolve the interfering reflections and treat this crystal as a non-merohedral twin. However, even with the use of a long detector-to-crystal distance and high-angle data, we still failed to cleanly separate partly overlapped reflections and to index the four components with four independent orientation matrices (*GEMINI*; Bruker, 1999). We hence resorted to the same techniques for data reduction as for the first crystal. For both crystals, the program *SADABS* (Sheldrick, 1996) was used to correct the data for absorption and inhomogeneity of the X-ray beam.

3. Twinning

As a first approximation, each crystal was considered to be a single crystal and a triclinic unit cell was determined using the *INDEX* procedure of the *SMART* program (Bruker, 2000*b*). Several alternative unit-cell options were suggested by the *BRAVAIS* option, some of which are presented in Table 1 for the first crystal, where column 1 corresponds to the original unit cell. The unit cells (1)–(4) are almost equal in geometry, but differ in spatial orientation. In the last column of Table 1, one more option of an orthorhombic I-centered unit cell is presented. Similar results were obtained for the second crystal. As will be shown below, the twin laws can be derived from the $\frac{2\,2\,2}{mmm}$ symmetry of the pseudo-orthorhombic supercell, defining a four-component twin.

In Fig. 2, the original unit cells (1) are shown in black, the pseudo-orthorhombic supercells (5) in blue and the orientation of the respective twin-unit cells (2), (3) and (4) in red, superimposed on five layers of lattice points. The pseudo-orthorhombic supercell (5) can be derived from the original triclinic cell (1) as follows: $\mathbf{a}_o = \mathbf{a}_{1t}$, $\mathbf{b}_o = \mathbf{b}_{1t}$ and $\mathbf{c}_o = \mathbf{a}_{1t} + \mathbf{b}_{1t} + 2\mathbf{c}_{1t}$. With $\mathbf{c}_o$ being approximately normal to the $\mathbf{a}_{1t}\mathbf{b}_{1t}$ plane. Rotation about each of the twofold axes intrinsic in the holohedry of the pseudo-supercell ($2\|\mathbf{a}_o$, $2\|\mathbf{b}_o$, $2\|\mathbf{c}_o$) relates the original triclinic cell to the respective twin cell:

(i) Fig. 2(*a*) illustrates that a 180° rotation of cell (1) around $\mathbf{a}_o$ or $\mathbf{a}_{1t}$ produces cell (2)

$$\mathbf{a}_{2t} = \mathbf{a}_{1t}, \quad \mathbf{b}_{2t} = -\mathbf{b}_{1t}, \quad \mathbf{c}_{2t} = -\mathbf{a}_{1t} - \mathbf{c}_{1t}.$$

(ii) Fig. 2(*b*) shows the 180° rotation of cell (1) around $\mathbf{b}_o$ or $\mathbf{b}_{1t}$ producing cell (3)

$$\mathbf{a}_{3t} = -\mathbf{a}_{1t}, \quad \mathbf{b}_{3t} = \mathbf{b}_{1t}, \quad \mathbf{c}_{3t} = -\mathbf{b}_{1t} - \mathbf{c}_{1t}.$$

(iii) Fig. 2(*c*) demonstrates a 180° rotation of cell (1) about $\mathbf{c}_o$ (normal to $\mathbf{a}_{1t}\mathbf{b}_{1t}$) resulting in cell (4)

$$\mathbf{a}_{4t} = -\mathbf{a}_{1t}, \quad \mathbf{b}_{4t} = -\mathbf{b}_{1t}, \quad \mathbf{c}_{4t} = \mathbf{a}_{1t} + \mathbf{b}_{1t} + \mathbf{c}_{1t}.$$

Concomitant with the four orientations of the unit cell within the same crystal, the indices for the faces of the crystal are not necessarily unique and care must be taken when describing the orientation of a crystal based on solely crys-

tallographic assignments. For example, while the (001) or (00$\bar{1}$) faces coincide for all fourling components, the ($\bar{1}$00) plane in the orientation of cell (1) overlaps with the ($\bar{1}$00) plane of cell (3), but corresponds to (10$\bar{1}$) for the orientation of cell (2) and to ($\bar{1}$01) for cell (4).

As mentioned above, the structures of the two different crystals were solved by direct methods in a single-crystal approximation and refined in the same approximation with the *SHELXTL* package to *R* indices of *ca* 0.20. Using the twin laws derived above, the structural models for the two crystals were subsequently refined as four-component twins using the procedure associated with the *HKLF* 5 format for merohedral twins in *SHELXTL*. Fractional contributions k_1, k_2, k_3, k_4 of the twin components were refined constraining $k_1 = 1 - k_2 - k_3 - k_4$. An *HKLF* 5 format data file was created where each line contained h, k, l, F_o^2, $\sigma(F_o^2)$, m, where m is the twin component number associated with the above derived cell (1), cell (2), cell (3) and cell (4). Thus, four lines of the data file correspond to each measured reflection

$$h, k, l, F_o^2, \sigma(F_o^2), -1$$
$$h, -k, -h-l, F_o^2, \sigma(F_o^2), -2$$
$$-h, k, -k-l, F_o^2, \sigma(F_o^2), -3$$
$$-h, -k, h+k+l, F_o^2, \sigma(F_o^2), 4.$$

The successful refinement of this model is shown in Table 2 and discussed in §4. The ratio of the volumes of the fourling domains refine to 55:9:20:16 for the first crystal and 27:19:29:25 for the second crystal.[3]

As an additional confirmation of this result, both structures have also been refined as four-component twins using *JANA*2000 (Petricek *et al.*, 2000). No significant differences were found, the ratios of the twin components agreeing to within 1%.

The structures of both twinned crystals were refined to low *R* indices of *ca* 0.04. All structural parameters for the two crystals are in excellent agreement. The atomic displacement parameters were considered to be anisotropic for all the atoms except H atoms; these were constrained to idealized positions with the N—H bonds on the external bisector of the *X*—N—*Y* (*X*, *Y* = C, N) angle, N—H distances of 0.86 Å and fixed isotropic displacement parameters of 0.04 Å^2.[4] The geometrical parameters obtained for the first crystal from the *SHELXTL* refinement for the four independent molecules as well as those obtained for the β-phase are compared in Table 3. The hydrogen-bond parameters are reported in Table 4.

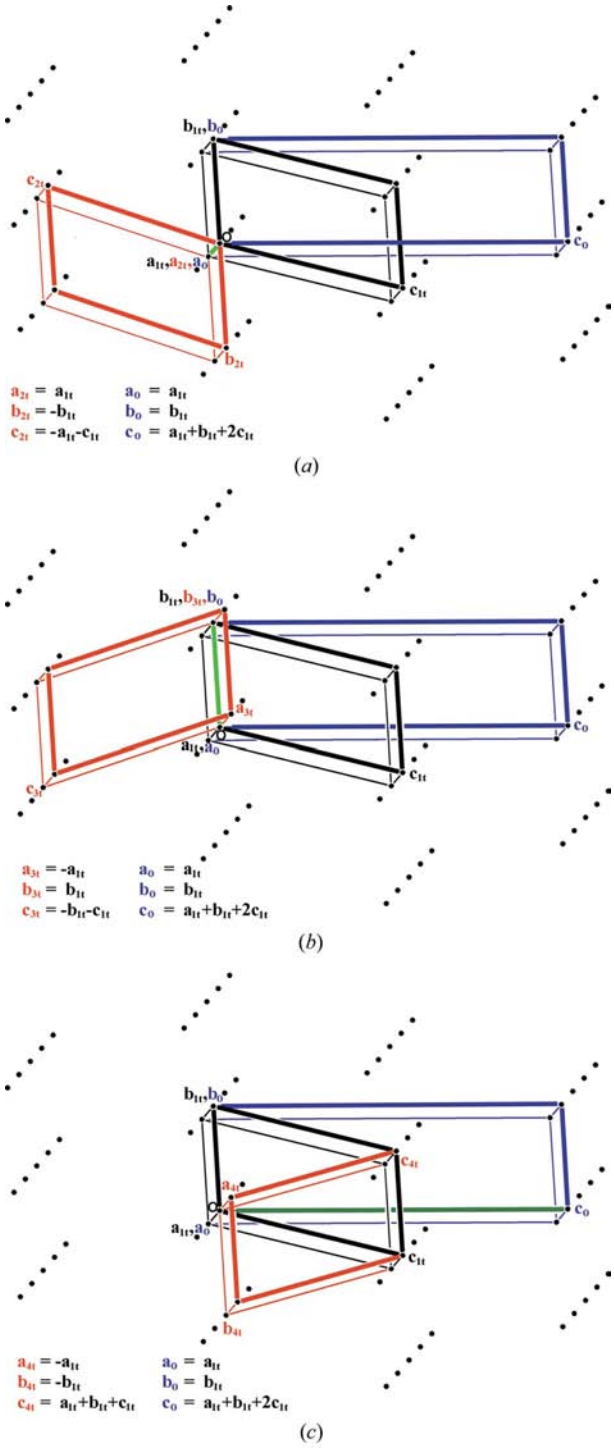

Figure 2
Twin rotations of α-NTO: 180° around the (*a*) $\mathbf{a}_o$, (*b*) $\mathbf{b}_o$ and (*c*) $\mathbf{c}_o$ axes. The original triclinic unit cell is shown in black, the pseudo-orthorhombic supercell in blue and the transformed cell in red.

4. Results and discussion

The crystal structure of α-NTO is triclinic, space group $P\bar{1}$. The unit-cell values are in good agreement with those reported by Lee & Gilardi (1993). It is satisfying that two programs, *SHELXTL* and *JANA*2000, give the same relative volumes of the twin components; one fourling component of the first crystal represents about 55% of the crystal volume with 9, 20 and 16% for the other components completing the total crystal volume. As a result, the orientation matrix and unit-cell parameters of the first crystal, which are determined from the

[3] We thank one of the referees for pointing out that the major component should have the positive batch number to obtain better values for the Fourier and variance calculations. However, testing this effect for crystal 1 produced insignificant changes, *e.g.* 0.03 e Å^{-3} in the final $\Delta\rho_{max}$.
[4] Supplementary data for this paper are available from the IUCr electronic archives (Reference: SN5022). Services for accessing these data are described at the back of the journal.

Table 3
Bond lengths (Å) and angles (°) for α-NTO.

	Molecule (1)	Molecule (2)	Molecule (3)	Molecule (4)	β-NTO[a]
N1—C5	1.283 (3)	1.288 (3)	1.283 (3)	1.280 (3)	1.290 (4)
N1—N2	1.358 (3)	1.373 (3)	1.365 (3)	1.378 (3)	1.366 (4)
N2—C3	1.367 (3)	1.357 (3)	1.355 (3)	1.356 (3)	1.369 (4)
C3—O3	1.220 (3)	1.228 (3)	1.223 (3)	1.220 (3)	1.228 (4)
C3—N4	1.377 (3)	1.374 (3)	1.386 (3)	1.389 (3)	1.373 (4)
N4—C5	1.348 (3)	1.343 (3)	1.348 (3)	1.341 (3)	1.352 (4)
C5—N5	1.454 (3)	1.443 (3)	1.444 (3)	1.440 (3)	1.440 (4)
N5—O5	1.217 (3)	1.223 (3)	1.216 (3)	1.220 (3)	1.212 (3)
N5—O6	1.217 (3)	1.208 (3)	1.224 (3)	1.217 (3)	1.226 (3)
C5—N1—N2	102.7 (2)	101.7 (2)	102.6 (2)	102.3 (2)	102.6 (2)
N1—N2—C3	112.8 (2)	113.9 (2)	113.5 (2)	113.5 (2)	113.0 (3)
O3—C3—N2	128.8 (2)	129.6 (2)	129.4 (2)	129.2 (2)	127.0 (3)
O3—C3—N4	127.4 (2)	127.7 (2)	127.5 (2)	128.2 (2)	129.5 (3)
N2—C3—N4	103.7 (2)	102.7 (2)	103.1 (2)	102.6 (2)	103.5 (3)
C5—N4—C3	105.5 (2)	106.9 (2)	106.1 (2)	106.8 (2)	106.4 (2)
N1—C5—N4	115.2 (2)	114.8 (2)	114.7 (2)	114.8 (2)	114.6 (3)
N1—C5—N5	121.9 (2)	121.7 (2)	122.0 (2)	122.6 (2)	122.2 (3)
N4—C5—N5	122.8 (2)	123.5 (2)	123.3 (2)	122.6 (2)	123.1 (2)
O5—N5—O6	126.5 (2)	126.1 (2)	126.9 (2)	127.2 (2)	125.7 (3)
O5—N5—C5	116.5 (2)	114.6 (2)	116.4 (2)	116.0 (2)	117.1 (3)
O6—N5—C5	117.0 (2)	119.2 (2)	116.7 (2)	116.8 (2)	117.2 (3)

References: (*a*) Bolotina *et al.* (2003).

intensity-weighted reflection centroids of the observed diffraction profiles, are more often dominated by the major twin component. This suggests that the unit-cell parameters determined for crystal (1) are more reliable than for crystal (2) where the four twin components are approximately equal in size, making up 27, 19, 29 and 25% of the crystal volume. Owing to the almost equal volumes of the four twin components in crystal (2), a deceptively low $R_{\rm merge}$ of 0.040 was obtained when averaging the data using orthorhombic symmetry [*cf.* 0.158 for crystal (1)].

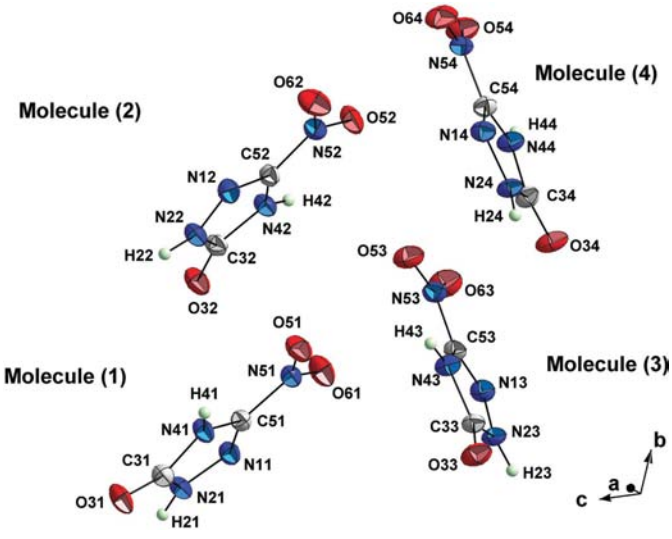

Figure 3
Asymmetric unit of α-NTO with 50% probability ellipsoids. The second digit in the name of each atom corresponds to the number of the molecule.

In Fig. 3, the four independent molecules in the asymmetric unit and their relative orientations are shown. The second digit in the name of each atom corresponds to the number of the molecule. All the molecules are planar, the largest deviations of the atoms in the five-membered rings from their least-square planes being 0.002 (1), 0.002 (1), 0.002 (1) and 0.004 (1) Å. The dihedral angles between these planes and the planes of the NO_2 groups are 1.5 (5), 2.4 (5), 1.1 (4) and 3.9 (4)° for molecules (1), (2), (3) and (4), respectively. Molecules (1) and (2) as well as (3) and (4) are almost parallel to one another with dihedral angles based on the complete molecules of 1.85 (7) and 2.95 (4)°, but the ribbons formed by these two pairs (see below) are non-parallel thus forming a dihedral angle of *ca* 70° with each other.

The most striking feature of the α-NTO crystal structure is seen in Fig. 4. Infinite flat ribbons of hydrogen-bonded molecules are formed parallel to **a**. There are two independent ribbons, one formed from molecules (1) and (2), and the other from molecules (3) and (4). For all four individual chains, molecules are joined by N1*x*···H4*x* and O3*x*···H2*x* (*x* = molecule number) hydrogen bonds. The N1*x*···H4*x* distances are 2.20, 2.19, 2.22 and 2.23 Å and those for O3*x*···H2*x* are 2.51, 2.52, 2.51 and 2.52 Å, for chains 1, 2, 3 and 4, respectively.[5] The 1,2 and the 3,4 flat chains are joined into ribbons by interchain O3*x*···H2*y* interactions, all of these hydrogen bonds being parallel to each other (Fig. 4). With corresponding distances of 2.04, 2.01 (ribbon 1,2) and 2.01, 2.01 Å for (ribbon 3,4) the hydrogen bonds between chains building the ribbons are significantly stronger than the hydrogen bonds creating the infinite chains along **a**. The β-phase (Lee & Gilardi, 1993; Zhurova & Pinkerton, 2001; Bolotina *et al.*, 2003) is also composed of planar molecules ($P2_1/c$, $Z = 4$). In this case, the planar molecules form puckered hydrogen-bonded layers parallel to *ab*, with four hydrogen bonds per molecule in contrast to the six observed here for the α-phase. Clearly, the additional hydrogen bonds in the α-phase are responsible for its higher density, 1.92 g cm^{-3} compared with 1.88 g cm^{-3} for the β-phase. The effect of hydrogen bonding of the carbonyl functional groups in the α-phase, the concomitant elongation of the C═O bond [1.220 (3), 1.228 (3), 1.223 (3), 1.220 (3) Å] compared with that obtained for the isolated molecule from gas-phase calculations (1.183–1.207 Å) and the resulting shift towards shorter frequency in the IR bands have been previously discussed (Hiyoshi *et al.*, 2004) – however, owing to the lack of structural data available for α-NTO, comparison was made to the crystalline β-NTO phase.

We may obtain additional insight into the twinning observed here by consideration of the ribbon stacking in the crystal. In Fig. 5 we present projections of the original cell

[5] No standard deviation is provided given that the distances are based on calculated positions of the H atoms.

Table 4
Hydrogen-bond lengths (Å) and angles (°) for α-NTO.

	H···A	D—H···A
N21—H21···O32^{i}	2.01	146.5
N21—H21···O31^{ii}	2.51	125.0
N41^{ii}—H41^{ii}···N11	2.20	140.6
N22^{iii}—H22^{iii}···O31	2.04	146.1
N22^{iii}—H22^{iii}···O32^{i}	2.52	125.8
N42^{i}—H42^{i}···N12^{iii}	2.19	141.9
N23—H23···O34^{iv}	2.01	147.4
N23—H23···O33^{ii}	2.51	123.4
N43^{ii}—H43^{ii}···N13	2.22	138.7
N24^{v}—H24^{v}···O33	2.01	147.4
N24^{v}—H24^{v}···O34^{iv}	2.52	123.5
N44^{iv}—H44^{iv}···N14^{v}	2.23	138.8

Symmetry codes: (i) $1-x,-y,2-z$; (ii) $-1+x,y,z$; (iii) $2-x,-y,2-z$; (iv) $-x,-y,1-z$; (v) $1-x,-y,1-z$. Distances and angles are based on H atoms fixed in idealized positions; N—H 0.86 Å and the H atoms are located on the external bisector of the X—N—Y (X,Y = C,N) angle.

(solid atoms) and the respective twin components (open atoms) in the same orientation as in Fig. 2. Molecules (1), (2), (3) and (4) are coloured green, red, blue and yellow, respectively. Potential twin boundaries are indicated by a dot/dash line. The hydrogen bonding between the molecular chains responsible for ribbon formation is indicated by hashed lines, the nitro groups being located at each end (compare Fig. 4). The structures obtained from the twin rotations about $\mathbf{a}_o$, $\mathbf{b}_o$ and $\mathbf{c}_o$, as derived mathematically from the coordinates of the molecules in the original cell and the appropriate transformation matrices, are presented in Figs. 5(*a*), (*c*) and (*e*).

In Fig. 5(*a*), we see that a 180° rotation of the structure about $\mathbf{a}_o$ produces an apparent continuation of the ribbon packing, *i.e.* the ribbons created by molecules (3) and (4) (blue–yellow) in the original packing are replaced by the same ribbons (blue–yellow) in the twin domain. However, ribbons (1,2) and (3,4) in the original cell are substituted by ribbons that propagate in the opposite direction with respect to $\mathbf{a}_{1t}$ – (1*,2*) and (3*,4*) – as required by the twofold rotation of the twin law. This reversal in the direction of the hydrogen-bonded ribbons can be visualized from Fig. 4.[6] Consequently, a twin interface perpendicular to the ribbon would result in the loss of the hydrogen-bonding stabilization energy, while the energy of the interaction between parallel ribbons at a stacking fault as indicated by the dot/dash line in Fig. 5(*a*) would be only slightly perturbed by this reversal. If the twin component is translated as in Fig. 5(*b*), we see an alternative twin boundary as indicated by the zigzag, dot/dash line. Again, there is a reversal of the ribbon directions while the ribbon face-to-face interactions are, in general, maintained. This suggests that growth of this twin component could evolve either from a plane parallel to *ab* or from a plane parallel to *ac*, with propagation from a plane perpendicular to **a** being disfavoured.

[6] The direction of the hydrogen bonds is defined as: chains with O3x^{ii}···H2x propagating in the direction of positive $\mathbf{a}_{1t}$: (1,2,3,4); chains propagating in the direction of negative $\mathbf{a}_{1t}$, as indicated by the O3x^{ii}···H2x direction: (1*,2*,3*,4*).

Fig. 5(*c*) illustrates original and twinned structures as observed after a 180° rotation of the unit cell about $\mathbf{b}_o$. Here, the application of the twin operation does not lead to an apparent flawless continuation of the ribbon packing. Instead, the rotated ribbons, *e.g.* formed by molecules 3 and 4 (open atoms, blue/yellow), line up parallel – in spite of the ∼ 70° angle usually found between ribbons – with the neighbouring original ribbons (1,2) (solid, green/red), leading to an obvious stacking fault as indicated by the dot/dash line. Fig. 5(*c*) also demonstrates how the orientation of the ribbons in the twinned domain again requires the interruption of the hydrogen bonds within the chains, if a twin interface should occur perpendicular to the ribbons. Again, this suggests twin propagation from a plane parallel to *ab* and not perpendicular to **a**. We note that removal of the first layer composed of blue/yellow ribbons from the twin, followed by an origin shift of the twin cell by $00\frac{1}{2}$ or $0\frac{11}{22}$ (Fig. 5*d*) produces a motif similar to Fig. 5(*b*). This would perhaps produce an energetically more favourable packing with the same conclusions with respect to crystal-growth directions of this component, as determined from Figs. 5(*a*) and (*b*).

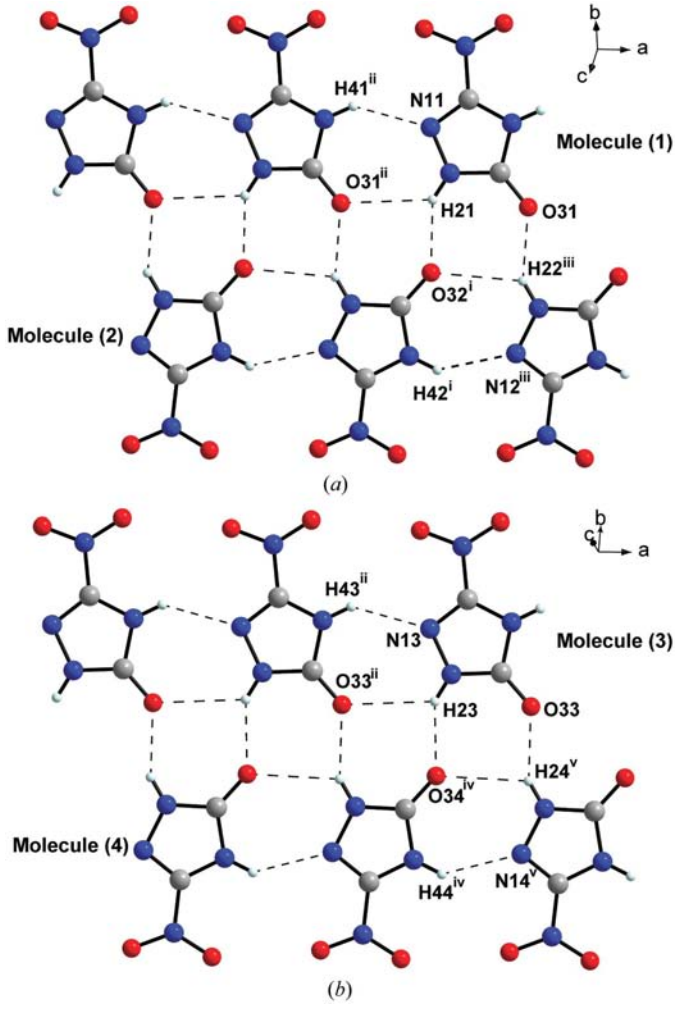

Figure 4
Planar hydrogen-bonded ribbons of α-NTO formed by molecules (*a*) 1,2 and (*b*) 3,4.

In Fig. 5(*e*), representing a 180° rotation about $\mathbf{c}_o$, the ribbon packing is very similar to that observed in Fig. 5(*c*). The twinning could originate again by the accidental ordering of a blue/yellow (3,4) ribbon parallel to the red/green ribbon (1,2) instead of at the 70° angle. The difference between these twinned structures (180° rotation about $\mathbf{b}_o$ and 180° rotation about $\mathbf{c}_o$) lies in the directionality of the hydrogen-bond propagation. Where ribbon (3,4) is positioned in Fig. 5(*c*), we find ribbon (3*,4*) in Fig. 5(*e*). As argued above, while a twin interface perpendicular to the ribbon faces seems unlikely for energetic reasons, a packing fault parallel to *ab* or between ribbon faces does not interrupt the hydrogen-bonding interactions. Removal of a ribbon followed by an origin shift leads to the same conclusions as above for a rotation about $\mathbf{b}_o$.

These conditions imply that all twin interfaces should be parallel to $\mathbf{a}_{1t}$, in particular, all three could occur at planes parallel to (010) or (001), (001) being a common face for all four unit-cell orientations (see Figs. 2 and 5). A publication reanalyzing the twins in terms of OD (order–disorder) theory is in preparation (Schwarzenbach, private communication).

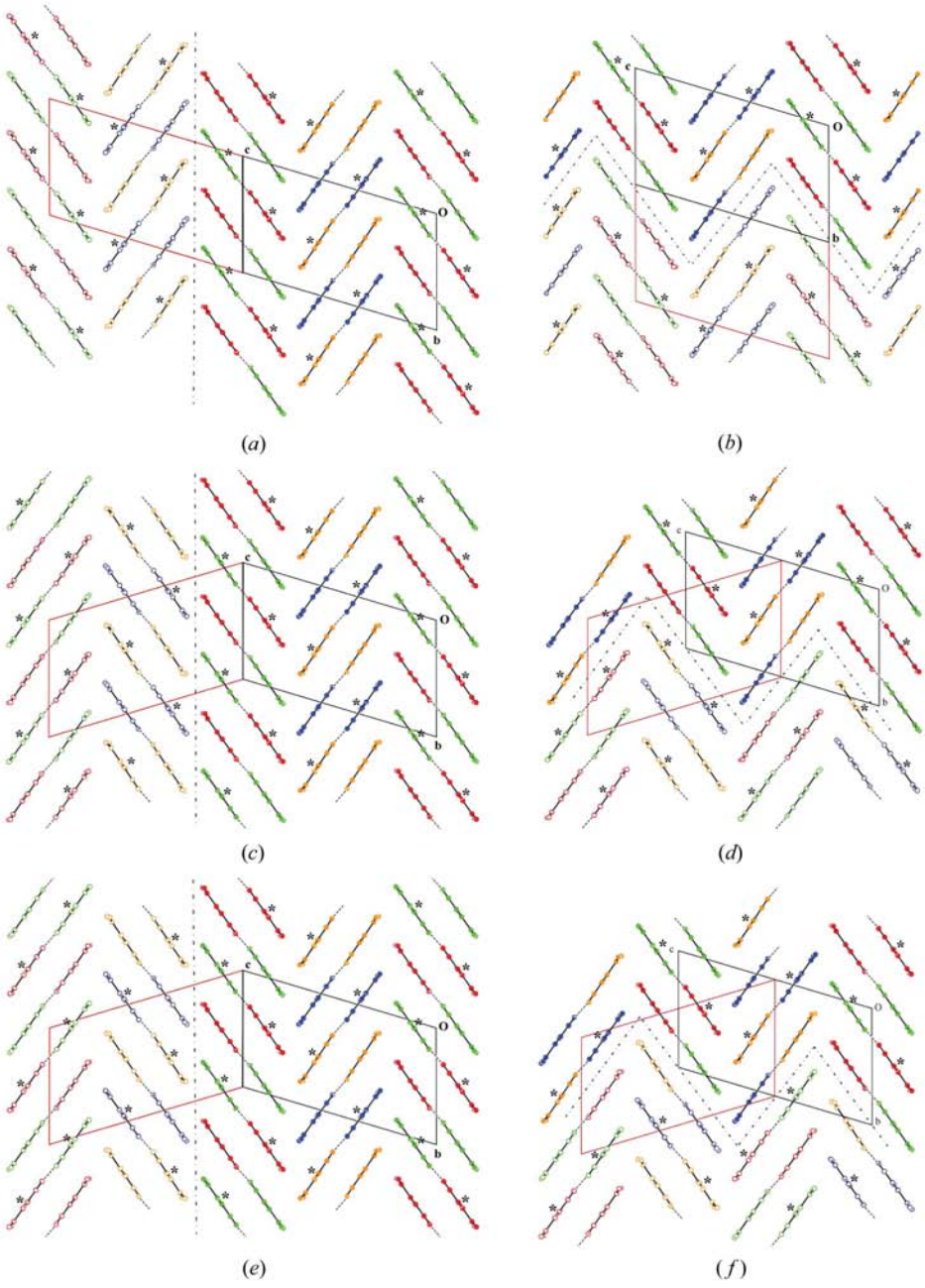

Figure 5
Twin components of the α-NTO crystal structure. (*a*) and (*b*), (*c*) and (*d*), and (*e*) and (*f*) represent the structure rotated through 180° around the $\mathbf{a}_o$, $\mathbf{b}_o$, $\mathbf{c}_o$ axis. Molecules 1, 2, 3 and 4 are colored green, red, blue and yellow, respectively. Asterisks indicate ribbons with an inverted direction of propagation. Solid atoms represent the original structure and open atoms correspond to the respective twin component. Dot/dashed lines indicate potential twin boundaries.

5. Conclusions

The predominant polymorph of the energetic material NTO, α-NTO, crystallizes as a four-component triclinic twin (fourling) with four crystallographically independent molecules in the asymmetric unit. Hydrogen bonding between these molecules creates two independent ribbons in the crystal structure. Twinning is probably initiated by the accidentally altered arrangement of one ribbon with respect to another one. The resulting twin laws can be rationalized as 180° rotations about the twofold axes of a pseudo-orthorhombic supercell. Energetic arguments make twin interfaces perpendicular to $\mathbf{a}_{1t}$ unlikely, but allow these stacking faults to occur at a plane parallel to (010) or (001). It is noteworthy that all the crystals examined in this work (as well as in

previous reports) were twinned, however, the relative amount of each twin component may vary.

We appreciate the financial support of the Office of Naval Research through contract number N00014-99-1-0392.

References

Beard, B. C. & Sharma, J. (1989). *J. Energ. Mater.* **7**, 181–198.
Bolotina, N. B., Zhurova, E. A. & Pinkerton, A. A. (2003). *J. Appl. Cryst.* **36**, 280–285.
Bruker (1999). *GEMINI*, Version 1.02. Bruker AXS Inc., Madison, Wisconsin, USA.
Bruker (2000*a*). *SHELXTL*, Version 6.1. Bruker AXS Inc., Madison, Wisconsin, USA.
Bruker (2000*b*). *SMART*, Version 5.622. Bruker AXS Inc., Madison, Wisconsin, USA.
Bruker (2001). *SAINT*, Version 6.28A. Bruker AXS Inc., Madison, Wisconsin, USA.
Cai, J.-G. & Deng, X. (2004). *Rengong Jingti Xuebao*, **33**, 18–23.
Chipen, G. I., Bokalder, R. P. & Grinshtein, V. Ya. (1966). *Khim. Geterotsiklicheskikh Soedinenii*, **2**, 110–116.
Franken, J., Hambir, S. A. & Dlott, D. D. (1999). *J. Appl. Phys.* **85**, 2068–2074.
Gehlen, H. & Schmidt, J. (1965). *Justus Liebigs Ann. Chem.* **682**, 123–135.
Gilardi, R. D. & Flippen-Anderson, J. L. (2002). *Acta Cryst.* A**58**, C232.
Heijden, A. E. D. M. van der (1998). *Curr. Top. Cryst. Growth Res.* **4**, 99–114.
Heijden, A. E. D. M. van der & Bouma, R. H. B. (2004). *Cryst. Growth Des.* **4**, 999–1007.
Hiyoshi, R. I., Kohno, Y. & Nakamura, J. (2004). *J. Phys. Chem. A*, **108**, 5915–5920.
Kim, K.-J. & Kim, K.-M. (2001). *Powder Technol.* **119**, 109–116.
Kofman, T. P., Pevzner, M. S., Zhukova, L. N., Kravchenko, T. A. & Frolova, G. M. (1980). *J. Org. Chem. USSR*, **16**, 375–378.
Kröger, C.-F., Miethchen, R., Frank, H., Siemer, M. & Pilz, S. (1969). *Chem. Ber.* **102**, 755–766.
Lee, K.-Y., Chapman, L. B. & Coburn, M. D. (1987). *J. Energ. Mater.* **5**, 27–33.
Lee, K.-Y. & Coburn, M. D. (1988). US Patent 4,733,610.
Lee, K.-Y. & Gilardi, R. (1993). *Mater. Res. Soc. Symp. Proc.* **296**, 237–242.
Manchot, V. W. & Noll, R. (1905). *J. Liebigs Ann. Chem.* **343**, 1–27.
Mathieu, J., Folly, P. & Bircher, H. R. (2001). Insensitive Munitions and Energetic Materials Technology Symposium. Bordeaux, France.
Petricek, V., Dusek, M. & Palatinus, L. (2000). *JANA*2000. Institute of Physics, Praha, Czech Republic.
Rothstein, L. R. & Petersen, R. (1979). *Propellants Explos.* **4**, 56–60.
Sheldrick, G. M. (1996). *SADABS*. University of Göttingen, Germany.
Singh, G. & Felix, S. P. (2002). *J. Hazard. Mater. A*, **90**, 1–17.
Singh, G. & Felix, S. P. (2003). *J. Mol. Struct.* **649**, 71–83.
Singh, G., Kapoor, I. P. S., Tiwari, S. K. & Felix, P. S. (2001). *J. Hazard. Mater. B*, **81**, 67–82.
Sorescu, D. C., Sutton, T. R. L., Thompson, D. L., Beardall, D. & Wight, C. A. (1996). *J. Mol. Struct.* **384**, 87–99.
Sorescu, D. C. & Thompson, D. L. (1997). *J. Phys. Chem. B*, **101**, 3605–3613.
Xiao, H.-M., Ju, X.-H., Xu, L.-N. & Fang, G.-Y. (2004). *J. Chem. Phys.* **121**, 12523–12531.
Zhurova, E. A. & Pinkerton, A. A. (2001). *Acta Cryst.* B**57**, 359–365.